10.1177/0003702817710248

Optical Properties of β-RDX Thin Films Deposited on Gold and Stainless Steel Substrates Calculated from Reflection–Absorption Infrared Spectra

José L. Ruiz-Caballero[1], Joaquín A. Aparicio-Bolaño[2], Amanda M. Figueroa-Navedo[1], Leonardo C. Pacheco-Londoño[1,3], and Samuel P. Hernandez-Rivera[1*]

[1]ALERT DHS Center of Excellence for Explosives Research, Department of Chemistry, University of Puerto Rico, Mayagüez, PR 00681, USA

[2]Department of Physics, University of Puerto Rico, Ponce, PO Box 7186, PR 00732, USA

[3]School of Basic and Biomedical Sciences, Simón Bolívar University, Barranquilla, Colombia

Corresponding author: Samuel P. Hernandez-Rivera, ALERT DHS Center of Excellence for Explosives Research, Department of Chemistry, University of Puerto Rico, Mayagüez, PR 00681, USA. Email: samuel.hernandez3@upr.edu; jose.ruiz9@upr.edu

ABSTRACT

The optical properties for crystalline films of the highly energetic material (HEM) hexahydro-1,3,5-trinitro-s-triazine, which is also known as RDX, deposited on gold (Au) and stainless steel (SS) substrates are presented. RDX has two important stable conformational polymorphs at room temperature: α-RDX and β-RDX. The optical properties obtained in the present work correspond to thin film samples of predominantly β-RDX polymorph. The infrared spectroscopic intensities measured showed significant differences in the β-RDX crystalline films deposited on the two

substrates with respect to the calculated real part of refractive index. The β-RDX/Au crystalline films have a high dynamic response, which is characterized by the asymmetric stretching mode of the axial nitro groups, whereas for the β-RDX/SS crystalline films, the dynamic response was mediated by the –N-NO_2 symmetric stretch mode. This result provides an idea of how the electric field vector propagates through the β-RDX crystalline films deposited on the two substrates.

Keywords: Reflection–absorption infrared spectroscopy, RAIS, Fourier transform infrared spectroscopy, FT-IR, optical constants, transverse optical vibration, ($\tilde{\nu}_{TO}$), longitudinal optical vibration, $\tilde{\nu}_{LO}$), film thickness.

INTRODUCTION

Interest in the study and characterization of α/β-RDX polymorphism has increased based on recent reports.[1–8] These investigations describe the crystallization phenomena under various deposition environments such as spin coating technology,[1] drop-on-demand inkjet technology,[2] changes in temperature and pressure,[3–6] and liquid inclusion phenomenon.[7] As is well known, in the solid state phase, the highly energetic material (HEM) cyclic nitramine hexahydro-1,3,5-trinitro-s-triazine (RDX)[9] preferentially conforms to the chair configuration of a six-membered ring (s-triazine or 1,3,5-triazine ring). The polymorphism exhibited by RDX is associated with the relative position of the three nitro (NO_2) groups in either equatorial or axial positions with respect to the s-triazine ring.[10] The α-RDX polymorph has been long established as the stable form at room temperature.[11] The orientations of the NO_2 groups in this case are two axial and one equatorial orientations, rendering a C_s symmetry to the conformation (axial-axial-equatorial RDX or AAE-RDX). The conversion from α-RDX to γ-RDX is theoretically demonstrated when the nitro groups change from

AAE-RDX to EEA-RDX, preserving the same symmetry.[12] The molecular conformation referred to as β-RDX has the NO_2 groups occupying all axial orientations with respect to the s-triazine ring (axial-axial-axial RDX or AAA-RDX) and a symmetry corresponding to C_{3v}.[13-15] There have been many reports in the scientific literature regarding RDX since its discovery in 1889 (by G. Henning, German Patent No. 104280). Initially, the use of RDX was based on its potential pharmacological properties. Presently, this compound is considered an essential ingredient for military shells, bombs, landmines, grenades, demolitions operations, and underwater blasting.[16] As part of the detection protocol, sensors require standards that can serve as target compounds such as HEMs with well-characterized properties to be validated. Since the discovery of RDX, numerous researchers have studied its physical and chemical properties,[17] but the RDX polymorphism of crystalline films prepared by deposition on substrates that can be used as samples and standards has received little attention.[2,18–21] Recently, we reported on the parameters of a spin-coating deposition methodology required to generate RDX crystalline films whose polymorphic distribution was favored by β-RDX.[1] Raman chemical images were carried out across a region of 40x40 μm (81 spectra) for SS substrates that were kept for over two years. Crystals of β-RDX were still present on the SS substrates. Goldberg and Swift were the first to confirm the stability of β-RDX.[8] Contributions along this line of effort by Wrable and co-workers[18] determined the residence time of RDX on various substrates. However, the optical properties (OP) have not been reported before using reflection–absorption infrared spectroscopy (RAIRS). Isbell and Brewster[22] obtained RDX optical constants using infrared (IR) transmission spectra.

Fourier transform IR (FT-IR) spectroscopy has vast applications in this area and provides the requirements necessary to characterize both ultrathin films (UTFs) and substrates. FT-IR spectroscopy has two important properties that offer practical advantages for the optical properties

characterization of thin films. First, it is one of a few techniques that can be used for in situ studies of chemical, physical, and biological processes on surfaces and at sample interfaces.[23–25] Second, it is highly useful in monitoring UTFs of absorbates for applications in fields such as optoelectronics and microelectronics of inorganic materials.[23] A UTF may be on the order of 100 nm (or slightly more). FT-IR spectroscopy has the sensitivity to analyze these films and even smaller thickness films. These films are usually known as monolayers. Finally, if FT-IR microspectroscopy itself does not provide the sensitivity to analyze thinner films, then a good alternative is to use reflection–absorption infrared spectroscopy coupled to FT-IR (FT-IR/RAIS).[26]

An in-depth knowledge of the optical properties of materials enables the development of devices for various applications in nanocircuits, molecular sensors, etc.[24] Optical properties also have great significance in energetic material research such as laser pyrolysis, laser-assisted combustion and ignition.[25] In the IR spectral region, optical properties are commonly obtained using two different approaches: measurements of transmission spectra, which are also used to identify the chemical structure by correlating the absorption peaks with the individual bonds and lattice vibrations, and measurements of reflection–absorption spectra. The latter is a very sensitive optical technique for measuring low concentrations of an absorbent material adhered to reflective surfaces.[27,28] It is possible to obtain the optical properties of the material under investigation from information contained in the reflection–absorption spectra of a material adhered to a given substrate. In addition, important aspects derived from material conductivity, such as the correlation between the electrical properties of the material and a specific optical property, are critical for sensor development applications.[29,30]

To determine the optical constants using FT-IR/RAIS, it is essential to previously obtain the following information on the experimental conditions: film thickness, relative intensity of IR

absorption bands, angle of incidence of the electromagnetic radiation, and electric field vector polarization state.[31] This last attribute is associated with the experiment setup and addresses the polarization of light and reflective mode in the experiments. The veracity of these suggestions is supported by the comparison of the findings of this study with those by other authors.[32] Several authors have formulated several equations in which these optical constants are calculated from the boundary condition problem derived from Maxwell equations.[27,28,33] After the exact model for an absorbate on a (highly reflective) metal substrate is identified, the correct equations must be selected to solve the problem on hand.

Several techniques can be used to measure the sample film thickness,[34,35] for example, (a) in vacuum: X-ray photoelectron spectroscopy (XPS), Auger electron spectroscopy (AES), and ion-based methods such as low-energy ion scattering (LEIS) and secondary ion mass spectrometry (SIMS); (b) ellipsometry via modeling of the optical constants; (c) the quartz crystal microbalance (QCM) method; and (d) atomic force microscopy (AFM). In the present work, AFM operated in the non-contact mode is the technique used to measure the sample thicknesses.

The theoretical foundations that can be used to determine the optical properties of layers of molecules deposited on surfaces are based on Maxwell's theory of electromagnetic radiation (EMR) of 1864.[36] Tolstoy, Chernyshova, and Skryshevsky[33] reformulated several of Maxwell's relevant equations that were used in this work. The approach focuses on the macroscopic property known as the permittivity of the medium ($\hat{\boldsymbol{\varepsilon}}$) to explain light phenomena such as propagation, absorption, reflection, and emission in matter.[37] The approach describes the collective excitations of the surface depending on the EMR source.[38,39] In this work, we adopt four premises. First, the vibrational modes of matter are excited in the IR region of the EMR spectrum. Second, because the magnetic permeability ($\hat{\mu}$) is practically zero in the optical frequencies of the IR window, the magnetic field

vector ($\vec{\mathbf{B}}$) can be considered as turned off because the interactions with the magnetic dipoles at these low frequencies are very small. Third, the medium considered hereby is the absorbent material. Finally, β-RDX crystalline films are isotropic. In addition, if the optical wave field is small compared to the electric field within atoms, it can be shown that the permittivity is independent of the magnitude of the electric field. A material that is exposed to an electric field vector $\vec{E}$ can be polarized by placing a polarizing plate in the path of the IR beam, thereby selecting two polarization states: parallel and perpendicular electric field orientations with respect to the plane of incidence of the light. Yamamoto and Ishida[37,40] and Tolstoy, Chernyshova, and Skryshevsky[33] express a relationship among the imaginary part of the permittivity (and its inverse), the film thickness (d), the incidence angle of the EMR (φ), the IR wavenumber $\tilde{\nu}$ (cm^{-1}), and the relative intensity of the reflected IR signal ($\Delta R/R$) as follows:

$$Im(1/\hat{\varepsilon}) \approx (\Delta R/R)_p/[8\pi d * \tilde{\nu} * (\sin\varphi)\,(\tan\varphi)] \quad \textbf{(1)}$$

$$Im(\hat{\varepsilon}) \approx (\Delta R/R)_S/[8\pi d * \tilde{\nu} * (\cos\varphi)] \quad \textbf{(2)}$$

where the subscript *s* ("senkrecht", perpendicular or s-polarization) indicates that the incident light is polarized at 90° with respect to the normal plane of incidence, denoted perpendicular polarization. The subscript *p* denotes parallel polarization (p-polarization) and represents light polarized at 0° with respect to the normal plane of incidence. The control of these states of polarizations is very important for the experimental setup used herein.[40] Because the EMR intensity is proportional to the square of $\vec{\mathbf{E}}$ (electric field strength), the ratio $\Delta R/R$ measures the reflectance change (ΔR) of the thin film deposited on the substrate with respect to the reflectance due to the clean substrate. It is important to emphasize that $(\Delta R/R)_S$ is inversely proportional to the angle of incidence, whereas $(\Delta R/R)_p$ has maximum values at grazing angles of incidence. Yamamoto and Ishida[37] refer to

functions $\mathrm{Im}(1/\hat{\varepsilon})$ and $\mathrm{Im}(\hat{\varepsilon}) = \varepsilon''$ as the transverse optical function and longitudinal optical function, respectively. The peak maximum of the function $\mathrm{Im}(\hat{\varepsilon})$ versus σ corresponds to σ_{TO}, whereas the maximum of $\mathrm{Im}(1/\hat{\varepsilon})$ corresponds to $\tilde{\nu}_{LO}$ vibrations of the medium. In conclusion, every optical equation is expressed as a function of the real part of the permittivity ($\varepsilon' = \mathrm{Re}(\hat{\varepsilon})$), imaginary part of the permittivity ($\mathrm{Im}(\hat{\varepsilon}) = \varepsilon''$), and imaginary part of the inverse of the permittivity ($Im(1/\hat{\varepsilon})$). Tolstoy, Chernyshova, and Skryshevsky[33] expressed this as:

$$Re[\hat{\varepsilon}(\tilde{\nu})] = \sqrt{(\varepsilon''(\tilde{\nu})/Im(1/\hat{\varepsilon})) - [\varepsilon''(\tilde{\nu})]^2} \quad \textbf{(3)}$$

$$Re[n(\tilde{\nu})] = \sqrt{\frac{1}{2}\left(\left(\sqrt{(\varepsilon'(\tilde{\nu}))^2 + (\varepsilon''(\tilde{\nu}))^2}\right) + \varepsilon'(\tilde{\nu})\right)} \quad \textbf{(4)}$$

$$k(\tilde{\nu}) = Im[n(\tilde{\nu})] = \sqrt{\frac{1}{2}\left(\left(\sqrt{(\varepsilon'(\tilde{\nu}))^2 + (\varepsilon''(\tilde{\nu}))^2}\right) - \varepsilon'(\tilde{\nu})\right)} \quad \textbf{(5)}$$

$$\alpha(\tilde{\nu}) = 2\pi\tilde{\nu}\, Im[\hat{\varepsilon}(\tilde{\nu})]/Re[(n(\tilde{\nu})] \quad \textbf{(6)}$$

where $Re[(n(\tilde{\nu})]$ is the real part of the refractive index, the $Im[n(\tilde{\nu})]$ is the imaginary part of the refractive index, and also known as the extinction coefficient. This last property describes absorption phenomena and is commonly known as the absorption coefficient α.

EXPERIMENTAL

Reagents

Acetone (CH_3COCH_3, HPLC+, 99.9%), methanol (CH_3OH, 99.9% HPLC grade), isopropyl alcohol ($CH_3CH(OH)CH_3$, 99.7%), and acetonitrile (CH_3CN, HPLC+, 99.9%) were acquired from Sigma-Aldrich Chemical Co. Standard solutions of RDX: 1000 ppm in acetonitrile and GC/MS primary standard grade were obtained from Restek Corp. and Chem Service, Inc., respectively. RDX was synthetized according to the Bachmann method with slight modifications.[41] Solvents and materials

for RDX synthesis: hexamethylenetetramine ($(CH_2)_6N_4$, 99% w/w) were purchased from Sigma-Aldrich Chemical Co. Sodium nitrite ($NaNO_2$, 99%) was purchased from Acros Organics. Fuming nitric acid (HNO_3, 97% w/w) and nitric acid (HNO_3, 70%, w/w) were purchased from Fisher Scientific International. Water used to prepare solutions, and clean and rinse glassware was deionized and doubly distilled (18 $M\Omega^{-1}cm^{-1}$) to make it HPLC grade. Stainless steel (SS) substrates (1.0 x 1.0 in^2) were purchased from Stainless Supply, Inc. Gold-coated standard microscope slides used as substrates (75 x 25 mm^2, 1 mm thickness) were acquired from Ted Pella, Inc.

Instrumentation and Experimental Setup

A spin-coating system (model 6800, Specialty Coatings Systems, Inc., Indianapolis, IN, USA) was used for the RDX sample deposition. The optical constants for both substrates were measured at 3000 revolutions per minutes (3k rpm). The ramp-up time was 2 s with a dwell time of 5 s, and the ramp-down time was 5 s with a dwell time of 0 s. Five seconds was a reasonable time to decrease the rotation frequency because it was sufficient to ensure higher sample hold down and avoid breaking the adhesion/cohesion surface forces of the film, thus preventing loss of uniformity by inertia. The spin coater interior was purged with highly filtered dry air. This was the same methodology as that reported previously to ensure reproducibility.[1]

A Bruker Optics IFS-66 v/s evacuable FT-IR interferometer was used for the mid-infrared (MIR) measurements. This system was equipped with a DGTS detector and accessories to measure the reflection and polarization of light. The IR spectral data in this work were analyzed using the Opus software suite (v.6.0, Bruker Optics). A variable angle reflection accessory model A 513/Q (Bruker Optics) was used for the measurements. All reflectance data were collected at 80° of incidence, which is reported as the most convenient and reproducible value for grazing angle

measurements.[1,26,42,43] The MIR polarizer was a model M 21-07/08 (Bruker Optics). The rotatable holder allowed an angular position of two angles of polarization with respect to the plane of incidence: perpendicular (s-polarized) and parallel (p-polarized). These polarization states of light are essential to characterize the optical properties in a reflective medium because they favor specific vibration modes. The area of analyzed samples was 1.0 x 1.0 in^2. FT-IR interferograms were collected in the 500–1800 cm^{-1} spectral range with nominal spectral resolution 4 cm^{-1}, 1000 scans for background and sample scans, and a scanner velocity of 4.0 kHz.

High-pressure liquid chromatography (HPLC) runs were performed in an Agilent 1100 series equipped with a C-18 column model Eclipse XDB platinum, 100 A, 5 µm, 150 mm by 4.6 mm (Grace-Alltech, Grace Discovery Sciences), and a variable wavelength detector, which was set to 254 nm. Borosilicate glass scintillation vials (Fisher Brand, Thermo-Fisher Scientific) sealed with Teflon screw caps and ultrasonic equipment were used to prepare the solutions. The solution preparation conditions were as follows: (a) 6 µL injection, (b) 0.7 mL flow rate, (c) 50% methanol/water, (d) column temperature of 27 °C, and (e) detector wavelength of 254 nm. These setup conditions enabled us to estimate the RDX standard solution purity from its synthesis.

An AFM (model Ntegra Spectra; NT-MDT America, Inc.) was used to characterize the topography, morphology, and thickness of the prepared coatings. The cantilever in the non-contact mode had a frequency of 340.95 kHz. Image Analysis software v.3.5.0.16646 (NT-MDT SPM Software), provided with the equipment, was used to evaluate the captured AFM images.

Preparation of Au Substrates

The RDX crystals (99.9%) were separately dissolved in two solvents: isopropyl alcohol to saturation (2.21×10^{-4} M) and acetone (2.00×10^{-1} M), as described in previous works.[1,17] Subsequently, the

substrates were cleaned and sonicated using acetone. Then, they were rinsed with distilled water and isopropyl alcohol. To ensure that no residual solvent persisted after washing, Raman spectra were collected. In the deposition, an aliquot of each solution (30 µL) was transferred to the substrate. Then, the spin coating routine was performed as previously described. Au substrates had an area of 1.0 x 1.0 in^2.

RESULTS AND DISCUSSION

AFM Characterization and Determination of the Surface Concentration

Thin film deposition by spin coating offers considerable advantages compared with methods such as: sample smearing[26] drop casting,[44] air spraying,[45] pneumatically assisted nebulization,[46] etc. It because is less subject to human error and provides a reliable coated surface for optical property studies.[47] An effective coating depends on both the operational parameters and the chemical properties of the adsorbate and substrate. The RDX crystalline films on SS substrates prepared with rapid spinning rates exhibit an increase in the ratio of α-RDX polymorph to β-RDX polymorph.[1] In fact, spin-coating deposition at 3000 rpm changes the α/β distribution and favors crystalline films of the less stable β-RDX.[1] The AFM measurements show that the mean height of the β-RDX crystalline films on SS substrates was 126 nm. A similar procedure at 3000 rpm generated β-RDX crystalline films deposited on the Au substrates. The morphological studies were accompanied by characterization with polarized RAIRS studies. The topography data for the β-RDX crystalline films on gold substrates deposited at 3k rpm are shown in Figure 1. This illustration shows fiber-like structures in the form of dendrites, as previously discussed for SS substrates.[1] This result was also confirmed by Raman spectroscopy measurements. From these results, the mean height was found to be 175 nm. The surface roughness was calculated using the reported equations for SS substrates.[1]

The purpose of this characterization is to estimate the film thickness (d, cm) in terms of the mean height for RDX crystalline films deposited on gold. These values are considered required input information for Eqs. 1 and 2.

An important finding is shown in Figure 2, where the unpolarized spectra of β-RDX crystalline films on Au substrate (β-RDX/Au) and SS substrate (β-RDX/SS) are compared. The most intense peak at ~1588 cm^{-1}, which is tentatively assigned to the asymmetric stretching of the nitro-axial group, was used for the calculations. The peak intensity of β-RDX/Au (from Figure 2a, blue trace) was 1.5-fold the intensity of β-RDX/SS (Figure 2b, red trace). This result corroborates that the thickness of β-RDX/Au was 1.4-fold that of β-RDX/SS. In other words, the peak intensity ratios prove the importance of using IR spectroscopy to obtain the optical properties. In addition, RAIRS can be used to study the distribution of different components in the matrices and surfaces throughout the sample.[46] Another relevant observation of Figure 2 is the presence of bands with similar intensities as the analyte (β-RDX) that can be identified as belonging to the solvent (acetone). These bands are labeled by using solid black guide arrows. Red dashed guide arrows are used to label bands tentatively assigned as overlap bands of RDX vibrational modes.[1] These bands show up as a result of the coexistence of the α-RDX and β-RDX polymorphs (6.6% and 93.4% relative abundance, respectively), as result of Stranski–Krastanov crystallization (confirmed by solvent-mediation theory).[1] The doublet near 1450 cm^{-1} has been tentatively assigned to CH_2 in-plane bending modes as belonging to the solvent coexisting with α-RDX.[1]

In another experiment, RDX was deposited on Au substrates using two solutions of markedly different concentrations. Samples were prepared using the described spin-coating deposition procedure. The concentrations of the solutions were as follows: 49 ppm RDX in isopropyl alcohol (or 2.2×10^{-4} M) and 2.0×10^{-1} M RDX in acetone. The unpolarized FT-RAIS spectra for the samples

after the spin-coating deposition of these solutions are shown in Figure 3. Raman spectroscopy was used to confirm the presence of β-polymorph in the RDX crystalline films on Au. The average thickness of the films based on the AFM measurements was 78 nm. The average thickness of the β-RDX/Au crystalline films obtained from the deposition of the 2.0 x 10^{-1} M RDX solution [Figure 3a, blue trace] was 2.24-fold larger than the corresponding thickness of β-RDX/Au crystalline films obtained from the deposition of the 2.21x10^{-4} M RDX solution [Figure 3b, red trace]. To further confirm this result, the same spectroscopic band (1588 cm^{-1}) was used to calculate the peak height intensity ratios. The peak height of β-RDX/Au crystalline films from 2.0x10^{-1} M was 2.27-fold that of β-RDX/Au crystalline films from 2.21x10^{-4} M. An important aspect of this contribution centered on estimating the thickness of β-RDX films upon sample deposition by spin coating on Au and SS substrates of the 2.0x10^{-1} M solution of RDX in acetone. In this respect, many challenging factors had to be controlled, such as the fast nucleation rate, shear forces, centrifugal forces, viscosity, Coriolis force, gravitational gradient, and fluid density. Figure 3 also shows the presence of the solvent vibrational bands indicated by solid black guide arrows. Possible overlap bands of α-RDX vibrational modes are illustrated by dashed red guide arrows.[1]

RAIS Measurements

The parameters used to obtain both $\mathrm{Im}(\hat{\varepsilon})$ and $\mathrm{Im}(1/\hat{\varepsilon})$ have been defined as follows: the sample thickness d and angle of incidence φ_1 of the EMR (80° with respect to the surface normal vector). In the RAIS experiments the spectral window of 1000–1800 cm^{-1} was used for the β-RDX crystalline films deposited on both substrates. This IR spectrum resulted from influences of both variables: the polarization state of the EMR field and incident angle of the radiation. In fact, the imaginary parts of the permittivity, refractive index, and wave vector were activated by these parameters. The RAIRS

spectrum of β-RDX/Au had higher intensity compared to β-RDX/SS, although both absorbates (β-RDX/Au and β-RDX/SS) were deposited under identical conditions of pressure, temperature, and spin-coating program. A plausible explanation for the reported intensity differences is the larger reflectivity of Au compared to SS.[27] These findings were corroborated by the AFM roughness measurements: the SS and Au substrates had average roughness values of 8 nm and 2 nm, respectively. Another important observation is related to the surface selection rules regarding the electric field vector: the observed IR signal intensities for p-polarized EMR were twice the s-polarized intensities.[27–31,34,36,38,39,43,48] An inspection of the FT-RAIS spectra for RDX clearly shows that this material is in the β-RDX conformation. The asymmetric stretching of the axial nitro group ($–NO_2$) was confirmed by the strongest band at 1587.2 $cm^{–1}$. Both asymmetric and symmetric in-plane bending of the $–CH_2–$ group from the s-triazine ring were evidenced by two peaks: one of higher intensity at 1444.5 $cm^{–1}$ and the other at 1421.3 $cm^{–1}$.[12,13] The peak at 1375 $cm^{–1}$ was attributed to the out-of-plane bending of the $–CH_2–$ group from the s-triazine ring. The symmetric stretching of $–N–NO_2$ was located at 1321.0 $cm^{–1}$. The band at 1269.0 $cm^{–1}$ was attributed to the $–N–NO_2$ stretching. Finally, the –N–C–N stretching of the s-triazine ring was located at 1224.6 $cm^{–1}$. These assignments were consistently confirmed on both substrates. The assignments are consistent with the results of Infante et al.,[11] who reported experimental data and theoretical calculations on $^{13}C–$ and $^{15}N–$ RDX isotopomers and the α-RDX → β-RDX phase transition monitored by Raman spectroscopy.[13] However, there are slight wavenumber shifts with respect to the values reported by Karpowicz et al.[14] and Karpowicz and Brill[14] for IR measurements of β-polymorph. These shifts can be attributed to the interactions with the surfaces on which the RDX was deposited. The interaction energies between absorbate and substrate must be further studied to confirm these observations. As

mentioned, β-RDX/Au and β-RDX/SS have different band intensities in the spectral range of 1420–1450 cm^{-1} because of the different optical properties in the MIR region.

Transversal and Longitudinal Optical Vibrations

The permittivity ($\hat{\varepsilon}$) is a macroscopic optical property of a medium, which is also very important at the atomic level and enables the description of the interaction of the electric field of an incident EMR wave with the medium.[38,39] The permittivity tensor characterizes the interactions of the electric field vector ($\vec{\mathbf{E}}$) with the absorbent matter. According to the previously presented mathematical description, the imaginary part of permittivity, which is symbolized as $\mathrm{Im}(\hat{\varepsilon}) = \varepsilon''$, is known as the longitudinal optical function. This function can be approximated using the relative intensity of the reflected MIR signal (ΔR/R), sample thickness (d), EMR angle of incidence to the sample surface (φ_1), and IR wavenumber ($\tilde{\nu}$). The real part of the permittivity (ε') can be determined from Eq. 1. The imaginary part of the permittivity can be calculated from Eq. 2. In addition, the peak maximum of the representation of the real part of the permittivity versus the wavenumber corresponds to the transversal optical vibration ($\tilde{\nu}_{\mathrm{TO}}$). The maximum representation of the imaginary part of the permittivity as a function of the wavenumber corresponds to the longitudinal optical vibration ($\tilde{\nu}_{\mathrm{LO}}$). Figure 4 shows a plot of ε versus $\tilde{\nu}$ for a β-RDX thin film deposited on an Au substrate. Representations of the real and imaginary components of the permittivity as functions of the wavenumber are included. The $\mathrm{Re}(\hat{\varepsilon})$ and $\mathrm{Im}(\hat{\varepsilon})$ peak maxima were at 1571.8 cm^{-1} and 1587.2 cm^{-1}, respectively. In this band, the asymmetric stretching of the axial nitro groups is activated as $\left(\mathrm{S}_{TO}\right)_{AU}$. This result is described by the peak maximum at 1587.2 cm^{-1} (Figure 4), which shows a high dynamic response of the asymmetric vibration mode of the axial nitro groups with respect to the

external electric field vector. In contrast, Figure 5 shows the β-RDX layers on SS substrates, where the peak maxima of $\mathrm{Re}(\hat{\varepsilon})$ and $\mathrm{Im}(\hat{\varepsilon})$ were 1315.3 cm^{-1}, and 1587.2 cm^{-1}, respectively. The results indicate two important aspects: (a) for both substrates, the transversal and longitudinal optical vibrations retain their peak maximum at 1587.2 cm^{-1}; (b) the external electric field vector can mediate the activation of the vibration mode of the axial nitro groups as a function of the substrate through the β-RDX layers.

The obtained $\mathrm{Re}(\hat{\varepsilon})$ and $\mathrm{Im}(\hat{\varepsilon})$ from the RAIS measurements of β-RDX crystalline films deposited on Au substrates $((\mathrm{Re}(\hat{\varepsilon}))_{\mathrm{RDX/Au}})$ suggest a high dynamic response, which is evidenced by the asymmetric vibration mode of the axial nitro groups with respect to the incident external electric field vector. However, the $\mathrm{Re}(\hat{\varepsilon})$ and $\mathrm{Im}(\hat{\varepsilon})$ obtained from β-RDX crystalline films deposited on SS substrates $((\mathrm{Re}(\hat{\varepsilon}))_{\mathrm{RDX/ss}})$ tend to indicate that the –N–NO_2 symmetric stretch vibration modes are involved in this assembly. Nevertheless, it is difficult to assign the presented optical behavior to a surface phenomenon such as a specific molecular surface orientation because this assignment requires further corroboration with theoretical models and other experiments. The main objective of this study is to develop, optimize, and validate a procedure for producing samples of β-RDX crystalline films on Au and SS substrates and characterize the corresponding chemical and physical properties. Specifically, in this contribution, the β-RDX crystalline films deposited on Au and SS substrates were characterized by RAIS.

Calculations of the Optical Constants for β-RDX/Au and β-RDX/SS

To characterize the interactions between RDX crystalline films (absorbing medium) and the incident electromagnetic wave, it is necessary to find information on (a) the permittivity $\hat{\varepsilon}$, (b) refractive index $\hat{n}$, and (c) wave propagation vector $\vec{k}$. However, these macroscopic properties are not directly

measurable. This work focuses on the behavior of optical constants when an absorbate (β-RDX crystalline film) is deposited on Au and SS substrates. The optical constants were graphed against the wavenumber σ of the incident EMR. Then, the resulting functions $n(\tilde{\nu})$, $k(\tilde{\nu})$, $\mathrm{Im}[\hat{\varepsilon}(\tilde{\nu})]$, and $\alpha(\tilde{\nu})$ were graphed against the reciprocal of lambda to generate the peak maxima. The online Supplemental Material contains Figures S3, S4, and S5 in which these optical constants are shown as function of wavenumber ($\tilde{\nu}$). Table I summarizes the information contained in Figures 3–6, where optical properties: $n(\tilde{\nu}) = \mathrm{Re}\left[n\left(\tilde{\nu}\right)\right], \kappa(\tilde{\nu}) = \mathrm{Im}\left[n\left(\tilde{\nu}\right)\right]$, and $\alpha(\tilde{\nu})$ were calculated. Two spectral windows in Figure 6: Region I (1300–1350 cm^{-1}), highlighted in light green and Region II (1550–1625 cm^{-1}), highlighted in light red. Table 1 shows the six maximum values of the real and imaginary parts of $n(\tilde{\nu})$ and $\kappa(\tilde{\nu})$ with respect to the substrates found in Regions I and II. In Table 2, two maximum values of $\mathrm{Im}[\hat{\varepsilon}(\tilde{\nu})]$ with respect to the substrate were obtained. These maxima were used to determine the nonzero optical conductivity (σ) for the absorbing media, which is theoretically determined by the following equation:

$$\sigma = \omega * \varepsilon_0 * \mathrm{Im}\left[\varepsilon\left(\tilde{\nu}\right)\right] \qquad (7)$$

where ω is the angular frequency (2πcν). The optical resistivity (ρ) of the absorbing media is the reciprocal of the optical conductivity.

The optical properties of energetic materials have been reported by Isbell and Brewster[22,25] and Yang et al.[32] The results in this contribution are more consistent with the results of Isbell and Brewster.[22,25] However, Figure 6 shows that this contribution was also consistent with the results of Yang et al.[32]: they have the same order of magnitude, although the experimental setups were markedly different. Table 3 summarizes the experimental details of the three methodologies used to

obtain the optical properties of RDX in the MIR region. Three different thicknesses were studied, but only the present contribution focused on thin RDX films. Finally, three angles of incidence were used to obtain the relevant information to calculate the desired optical properties. Moreover, this contribution includes two important aspects of the calculated optical constants: (i) the longitudinal and transverse optical vibrations are not mediated by the substrate; (ii) the real part of the refractive index, $\mathrm{Re}[n(\tilde{\nu})]$, behaves similar to the real part of the permittivity, $\mathrm{Re}[\hat{\varepsilon}(\tilde{\nu})]$.

Many differences appear in the ranges of 1250–1350 cm^{-1} and 1550–1625 cm^{-1} in Figure 6. In the range of the symmetric stretching of the nitro groups (1250–1350 cm^{-1}), both SS and ZnSe substrates shift the peak maxima. This result is in contrast to the behavior of the Au substrate, where the maximum peak appears in the region of the nitro group asymmetric stretching (1575.6 cm^{-1}), and no shifting was observed. As previously discussed, the maximum peaks of $\mathrm{Re}[n(\tilde{\nu})]$ and $\mathrm{Re}[\hat{\varepsilon}(\tilde{\nu})]$ are activated by both (a) the incident angle of infrared light traversing the RDX layer and (b) the type of substrate. Literature shows that some efforts have been directed to study the splitting of $\tilde{\nu}_{TO}$ and $\tilde{\nu}_{LO}$, which is also an interesting topic of discussion.[40] The authors concur that the splitting of bands arises from perturbations of the electric field owing to the induced dipole moments.[40] In fact, Yamamoto and coworkers[40] have mentioned in their conclusions that the shifts in peak position and changes in peak shapes may be because of the TO–LO splitting in the spectra at oblique angles of incidence.[39] The same observation was made by Tolstoy and coworkers.[33]

CONCLUSION

The RAIRS measurements were used to obtain the optical constants of predominantly β-RDX thin crystalline films deposited on Au and SS substrates. The theoretical equations required to calculate the optical properties of the thin films were effectively used to analyze the results of the MIR

measurements. The refractive index $[n(\tilde{\nu})]$, absorption coefficient $[\alpha(\tilde{\nu})]$, and absorption index $[k(\tilde{\nu})]$ of β-RDX films, which were calculated from the MIR-RAIS measurements, were consistent with the reported values in the literature, although the spectral range investigated in this contribution was much wider and the angle of incidence of the MIR radiation was much steeper. Considering that previous reports were not used to calculate the optical properties of a polymorphic energetic material (RDX) using RAIRS, these results intend to update the former. Regarding the contributions of the substrates to the optical properties of the adsorbate, these results can be attributed mainly to the reflectivity of the substrate. RAIS spectra of β-RDX are more intense and calculated optical constants are larger in magnitude for higher reflectivity Au. In addition, β-RDX (adsorbate) shows a response that intensifies both transversal ($\tilde{\nu}_{\mathrm{TO}}$) and longitudinal ($\tilde{\nu}_{\mathrm{LO}}$) optical vibrations. This sensitivity manifestation is depicted by $\tilde{\nu}_{\mathrm{TO}} = \tilde{\nu}_{\mathrm{LO}}$ for both substrates at 1587.2 cm^{-1}. $\tilde{\nu}_{TO}$ (or $\tilde{\nu}_{LO}$) becomes sensitive for β-RDX/Au (or β-RDX/SS) crystalline films through the asymmetric stretch of the axial $–NO_2$ groups. Furthermore, $\mathrm{Re}[\mathrm{n}(\tilde{\nu})]$ and $\mathrm{Re}[\hat{\varepsilon}(\tilde{\nu})]$ show similar behavior when β-RDX is deposited on SS and on Au, which splits the two maximum peaks in the 1250–1350 cm^{-1} and 1550–1625 cm^{-1} ranges.

ACKNOWLEDGMENTS

This material is based upon work supported by the Department of Homeland Security, Science and Technology Directorate, Office University Programs, under Grant Award 2013-ST-061-ED0001. Any opinions, findings, and conclusions or recommendations expressed in this material are those of the author(s) and do not necessarily reflect the views of the Department of Homeland Security.

REFERENCES

1. A.M. Figueroa-Navedo, J.L. Ruiz-Caballero, L.C. Pacheco-Londoño, S.P. Hernandez-Rivera. "Characterization of α- and β-RDX Polymorphs in Crystalline Deposits on Stainless Steel Substrates". Cryst. Growth. Des. 2016. 16(7): 3631-3638.

2. E.D. Emmons, M.E. Farrell, E.L. Holthoff, A. Tripathi, et al. "Characterization of Polymorphic States in Energetic Samples of 1,3,5-trinitro-1,3,5-triazine (RDX) Fabricated Using Drop-On-Demand Inkjet Technology". Appl. Spectrosc. 2012. 66(6): 628-635.

3. B.J. Baer, J. Oxley, M. Nicol. "The Phase Diagram of RDX (Hexahydro-1,3,5-trinitro-s-triazine) Under Hydrostatic Pressure". High Pressure Res. 1990. 2: 99-108.

4. P.J. Miller, S. Block, G.J. Piermarini. "Effects of Pressure on the Thermal Decomposition Kinetics, Chemical Reactivity and Phase Behavior of RDX". Combust. Flame. 1991. 83(2): 174-184.

5. P. Torres, L. Mercado, I. Cotte, S.P. Hernandez, et al. "Vibrational Spectroscopy Study of β- and α-RDX Deposits". J. Phys. Chem. B. 2004. 108(26): 8799-8805.

6. Z.A. Dreger, Y.M. Gupta. "Raman Spectroscopy of High-Pressure-High-Temperature Polymorph of Hexahydro-1,3,5-trinitro-1,3,5-triazine (ε-RDX)". J. Phys. Chem. A. 2010. 114(26): 7038-7047.

7. J.W. Kim, J.K. Kim, H.S. Kim, K.K. Koo. "Characterization of Liquid Inclusion of RDX Crystals with a Cooling Crystallization". Cryst. Growth Des. 2009. 9(6): 2700-2706.

8. I.G. Goldberg, J.A. Swift. "New Insights into the Metastable β Form of RDX". Cryst. Growth Des. 2012. 12: 1040-1045.

9. P.W. Cooper. Explosives Engineering. New York: Wiley-VCH, 1996.

10. W.C. McCrone. "Crystallographic Data. 32. RDX (Cyclotrimethylenetrinitramine)". Anal. Chem. 1950. 22(7): 954-955.

11. C.S. Choi, E. Prince. "The Crystal Structure of Cyclotrimethylenetrinitramine". Acta Cryst. B. 1972. 28(9): 2857-2852.

12. R. Infante-Castillo, L. Pacheco-Londoño, S.P. Hernandez-Rivera. "Vibrational Spectra and Structure of RDX and its 13C- and 15N-Labeled Derivatives: A Theoretical and Experimental Study". Spectrochim. Acta, Part A. 2010. 76(2): 137-141.

13. R. Infante-Castillo, L.C. Pacheco-Londoño, S.P. Hernández-Rivera. "Monitoring the α → β Solid–Solid Phase Transition of RDX with Raman Spectroscopy: A Theoretical and Experimental Stud". J. Mol. Struct. 2010. 970(1): 51-58.

14. R.J. Karpowicz, S.T. Sergio, T.B. Brill. "β-Polymorph of Hexahydro-1,3,5-trinitro-s-triazine. A Fourier Transform Infrared Spectroscopy Study of an Energetic Material". Ind. Eng. Chem. Prod. Res. Dev. 1983. 22(2): 363-365.

15. R.J. Karpowicz, T.B. Brill. "Comparison of the Molecular Structure of Hexahydro-1,3,5-Trinitro-S-Triazine in the Vapor, Solution and Solid Phases". J. Phys. Chem. 1984. 88(3): 348-352.

16. H.G. Gallagher, R.M. Vrcelj, J.N. Sherwood. "The Crystal Growth and Perfection of 2,4,6-Trinitrotoluene". J. Cryst. Growth. 2003. 250(3): 486-498.

17. G. Gillen, C. Zeissler, C. Mahoney, A. Lindstrom, et al. "Automated Analysis of Organic Particles Using Cluster SIMS". Appl. Surf. Sci. 2004. 231-232: 186-190.

18. M. Wrable-Rose, O.M. Primera-Pedrozo, L.C. Pacheco-Londoño, S.P. Hernandez-Rivera. "Preparation of TNT, RDX and Ammonium Nitrate Standards on Gold-on-Silicon Surfaces by Thermal Inkjet Technology". Sens. Imaging. 2010. 11(4): 147-169.

19. E. Windsor, M. Najarro, A. Bloom, B. Banner Jr., et al. "Application of Inkjet Printing Technology to Produce Test Materials of 1,3,5-Trinitro-1,3,5 Triazacyclohexane for Trace Explosive Analysis". Anal. Chem. 2010. 82(20): 8519-8524.

20. A.C. Ihnen, A.M. Petrock, T. Chou, P.J. Samuels, et al. "Crystal Morphology Variation in Inkjet-Printed Organic Materials". Appl. Surf. Sci. 2011. 258(2): 827-833.

21. J.R. Verkouteren, J. Lawrence, G.A. Klouda, M. Najarro, et al. " Performance Metrics Based on Signal Intensity for Ion Mobility Spectrometry–Based Explosive Trace Detectors Using Inkjet Printed Materials". Analyst. 2014. 139(21): 5488-5498.

22. R.A. Isbell, M.Q. Brewster. "Optical Properties of RDX and HMX". Mater. Res. Soc. Symp. Proc. 2011. 418: 85.

23. D.L. Allara, A. Baca, C.A. Pryde. "Distortions of Band Shapes in External Reflection Infrared Spectra of Thin Polymer Films on Metal Substrates". Macromolecules. 1978. 11(6): 1215-1220.

24. O.S. Heavens. "Thin Film Research Today". Nature. 1970. 228(5276): 1036-1039.

25. R.A. Isbell, M.Q. Brewster. "Optical Properties of Energetic Materials: RDX, HMX, AP, NC/NG, and HTPB". Propellants, Explos., Pyrotech. 1998. 23(4): 218-224.

26. O.M. Primera-Pedrozo, Y.M. Soto-Feliciano, L.C. Pacheco-Londoño, et al. "Detection of High Explosives Using Reflection Absorption Infrared Spectroscopy with Fiber Coupled Grazing Angle Probe/FTIR". Sens Imaging. 2009. 10(1): 1-13.

27. R.G. Greenler. "Infrared Study of Adsorbed Molecules on Metal Surfaces by Reflection Techniques". J. Chem. Phys. 1966. 44: 310

28. P.B. Johnson, R.W. Christy. "Optical Constants of the Noble Metals". Phys. Rev. B. 1972. 6(12): 4370

29. L.C. Pacheco-Londoño, W. Ortiz-Rivera, O.M. Primera-Pedrozo, S.P. Hernandez-Rivera. "Vibrational Spectroscopy Standoff Detection of Explosives". Anal. Bioanal. Chem. 2009. 395(2): 323-335.

30. N.J. Galan-Freyle, L.C Pacheco-Londoño, A.M. Figueroa-Navedo, S.P. Hernandez-Rivera. "Standoff Detection of Highly Energetic Materials Using Laser-Induced Thermal Excitation of Infrared Emission". Appl. Spectrosc. 2015. 69(5): 535-544.

31. R.G. Greenler, R.R. Rahn, J.P. Schwartz. "The Effect of Index of Refraction on the Position, Shape, and Intensity of Infrared Bands in Reflection-Absorption Spectra". J. Catal. 1971. 23(1): 42-48.

32. C.S.C. Yang, B.R. Williams, M.S. Hulet, R.W. Miles, et al. "Spectral Characterization of RDX, ETN, PETN, TATP, HMTD, HMX, and C-4 in the Mid-Infrared Region. ECBC-TR-1166". UNCLASSIFIED Report. Maryland: U.S. Army Edgewood Chemical Biological Center: Aberdeen Proving Ground, 2014.

33. V.P. Tolstoy, I.V. Chernyshova, V.A. Skryshevsky. Handbook of Infrared Spectroscopy of Ultrathin Films. New Jersey: John Wiley & Sons, Inc., 2003

34. A. Sengupta, S. Herminghaus, C. Bahr. "Liquid Crystal Microfluidics: Surface, Elastic and Viscous Interactions at Microscales". Liq. Cryst. Rev. 2014. 2(2):73-110.

35. A.O. Kivioja, A.-S. Jääskeläinen, V. Ahtee, T. Vuorinen. "Thickness Measurement of thin Polymer Films by Total Internal Reflection Raman and Attenuated Total Reflection Infrared Spectroscopy". Vib. Spectrosc. 2012. 61: 1-9.

36. J.C. Maxwell: A Treatise on Electricity and Magnetism. New York: Dover Publications, Inc., 1954.

37. K. Yamamoto, H. Ishida. "Optical Theory Applied to Infrared Spectroscopy". Vib. Spectrosc. 1994. 8(1): 1-36.

38. C. Kittel. Introduction to Solid State Physics. Eighth ed. New Jersey: Wiley, 2004.

39. N.W. Ashcroft, N.D. Mermin. Solid State Physics. Florida: Harcourt, Inc., 1976.

40. K. Yamamoto, H. Ishida. "Interpretation of Reflection and Transmission Spectra for Thin Films: Reflection". Appl. Spectrosc. 1994. 48(7): 775-787.

41. W.E. Bachmann, J.C. Sheehan. "A New Method of Preparing the High Explosive RDX". J. Am. Chem. Soc. 1949. 71(5): 1842-1845.

42. P. Hollins, J. Pritchard. "Infrared Studies of Chemisorbed Layers on Single Crystals". Prog. Surf. Sci. 1985. 19(4): 275-349.

43. R.G. Greenler. "Design of a Reflection–Absorption Experiment for Studying the IR Spectrum of Molecules Adsorbed on a Metal Surface". J. Vac. Sci. Technol. 1975. 12: 1410.

44. C.H. Liu, X. Yu. "Silver Nanowire-Based Transparent, Flexible, and Conductive Thin Film". Nanoscale Res. Lett. 2011. 6:75

45. Y.C. Lu, K.S. Chou. "Tailoring of Silver Wires and Their Performance as Transparent Conductive Coatings". Nanotechnology. 2010. 21(21): 215707-215713.

46. M.A. Barreto-Cabán, L.C. Pacheco-Londoño, M.L. Ramírez, S.P. Hernández-Rivera. “Novel Method for the Preparation of Explosive Nanoparticles”. Proc. SPIE. 2006. 6201: 620129-620139.

47. M. Chwastek, J. Weszka, J. Jurusik, B. Hajduk, et al. "Influence of Technological Conditions on Optical Properties and Morphology of Spin-Coated PPI Thin Films". Arch. Mater Sci. Eng. 2011. 48(2): 69-76.

48. L.C. Pacheco-Londoño, A. Santiago, J. Pujols, O.M. Primera-Pedrozo, et al. "Characterization of Layers of Tetryl, TNB and HMX on Metal Surfaces Using Fiber Optics Coupled Grazing Angle-FTIR". Proc. SPIE. 2007. 6542: 1-3. doi: 10.1117/12.720976

10.1177/0003702817710248

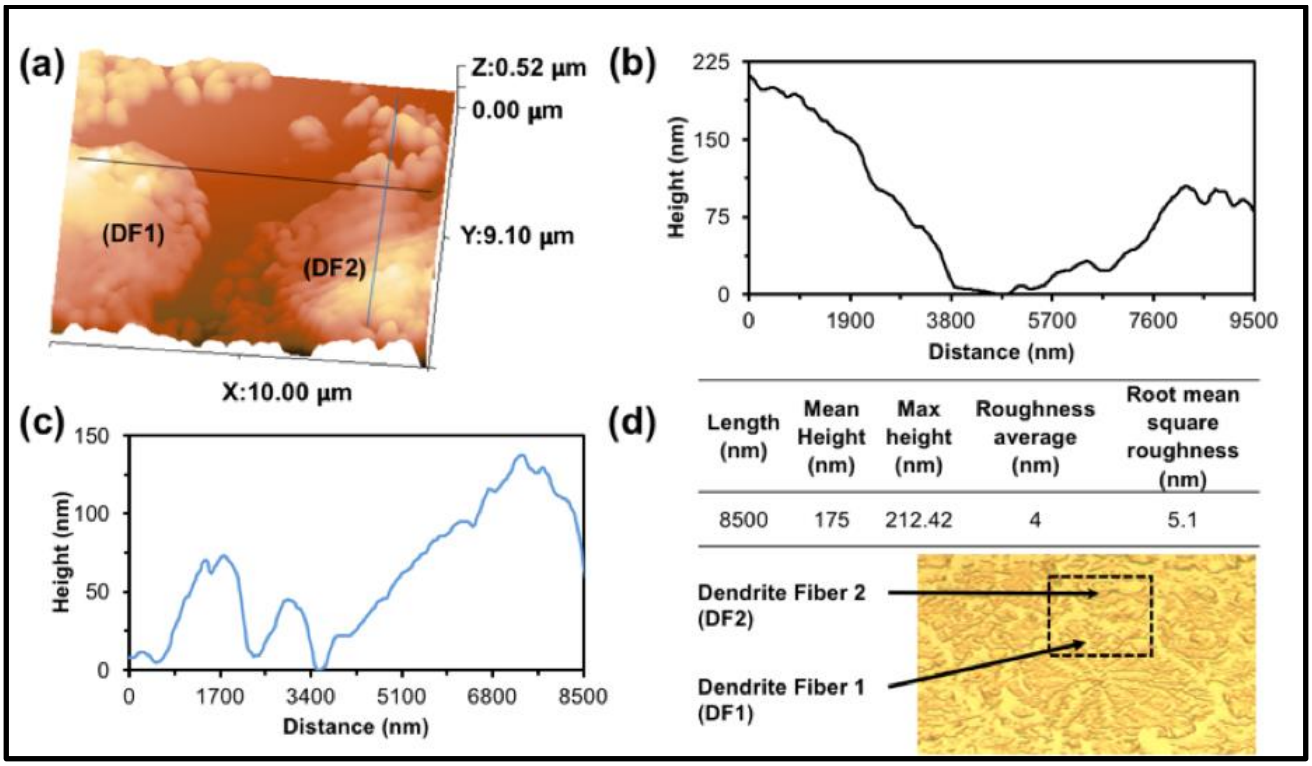

Figure 1. AFM image and analysis of predominantly β-RDX dendrite fibers (DF1 and DF2) formed at 3k rpm on Au substrates: (a) topological imaging; (b) height profile of the horizontal line (black); (c) height profile of the fibers (DF2) along the vertical line (blue); (d) fiber dimensions determined from (b) and (c).

10.1177/0003702817710248

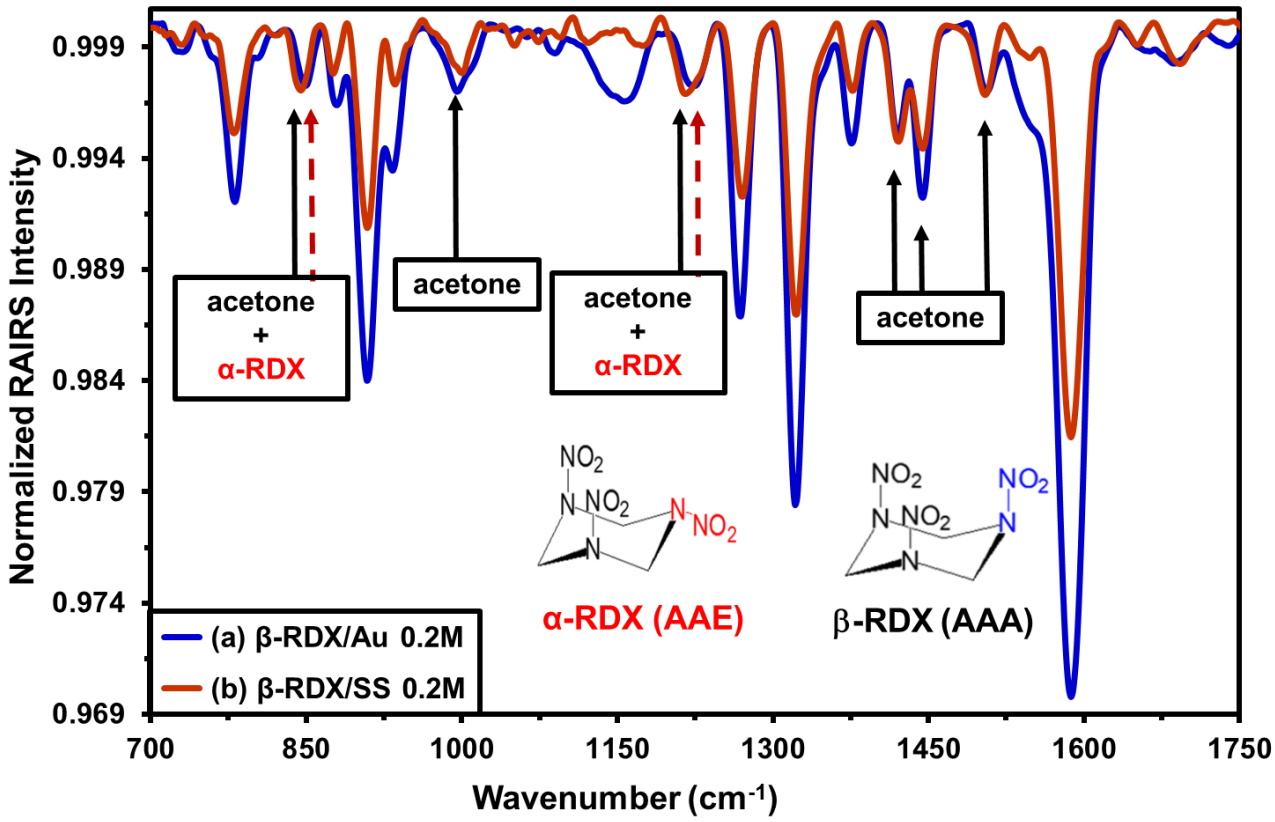

Figure 2. Unpolarized RAIRS spectra of predominantly β-RDX crystalline films on (a) Au substrates (blue trace) and (b) SS substrates (red trace). Solvent modes are presented with solid arrow, and the dashed arrows represent concomitant vibrational modes of the solvent and remaining α-RDX polymorph.

10.1177/0003702817710248

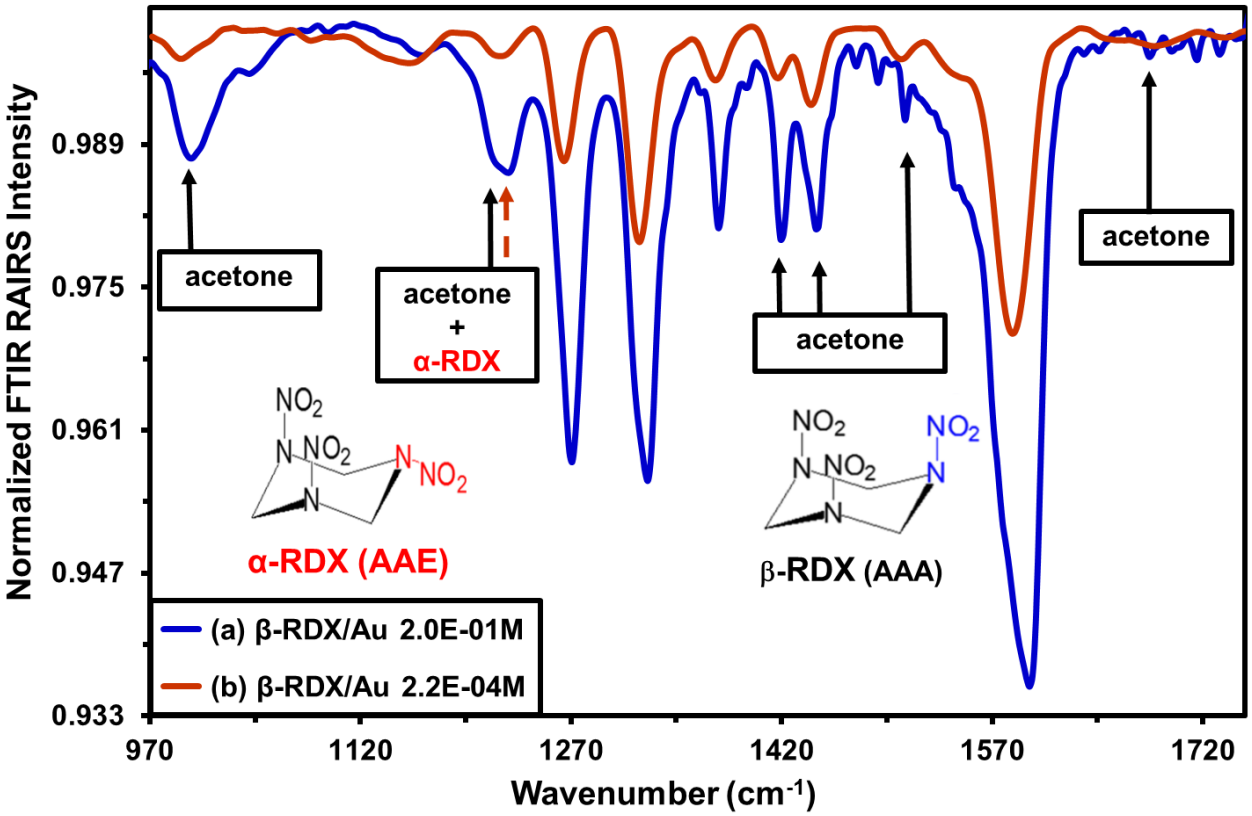

Figure 3. Unpolarized RAIRS spectra of predominantly β-RDX crystalline films on Au substrates at two concentrations: (a) 2.0×10^{-1} M (blue line) and (b) 2.2×10^{-4} M (red line). Solvent modes are presented with solid arrows and concomitant vibrational modes between solvent and remaining α-RDX polymorph are pointed with red dashed arrows.

10.1177/0003702817710248

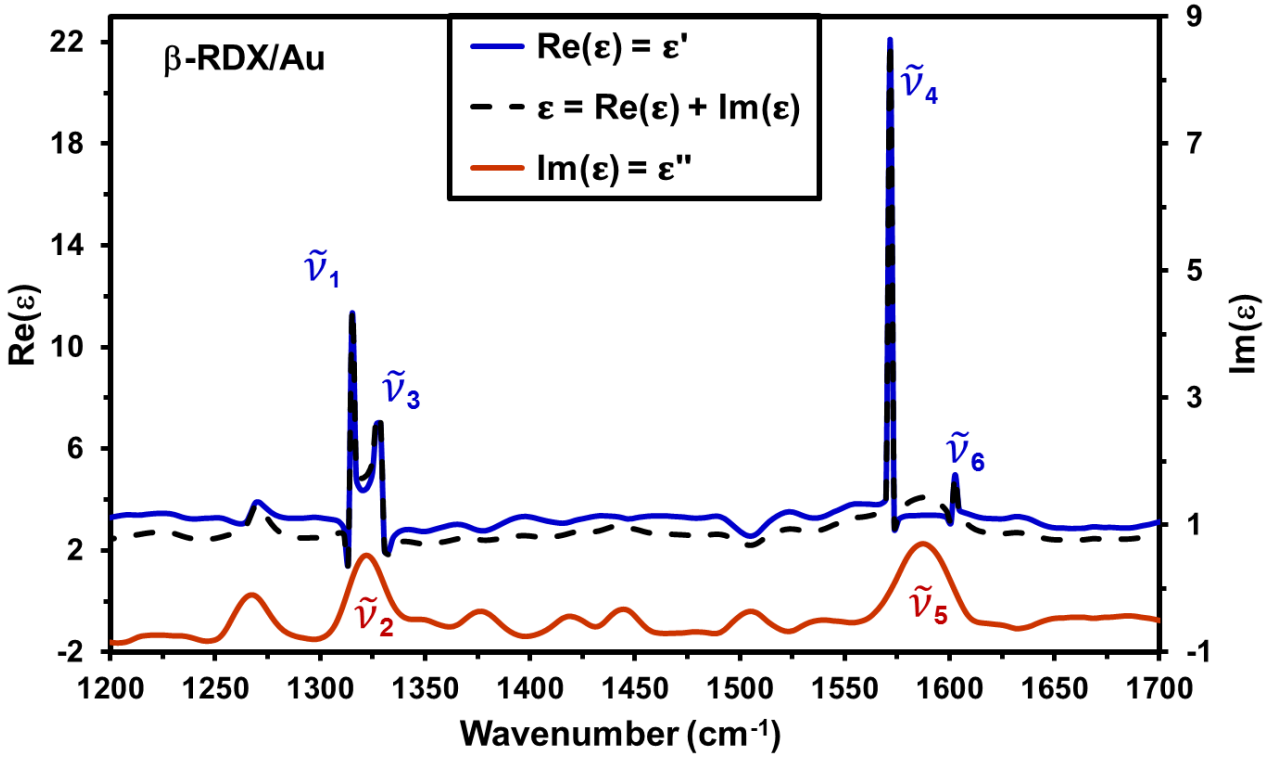

Figure 4. Permittivity (ε) of predominantly β-RDX crystalline films deposited on Au substrates (segmented black line). The transversal optical function is expressed as the imaginary part [Im(ε̂); red trace] and real part [Re(ε̂); blue trace] of the permittivity.

10.1177/0003702817710248

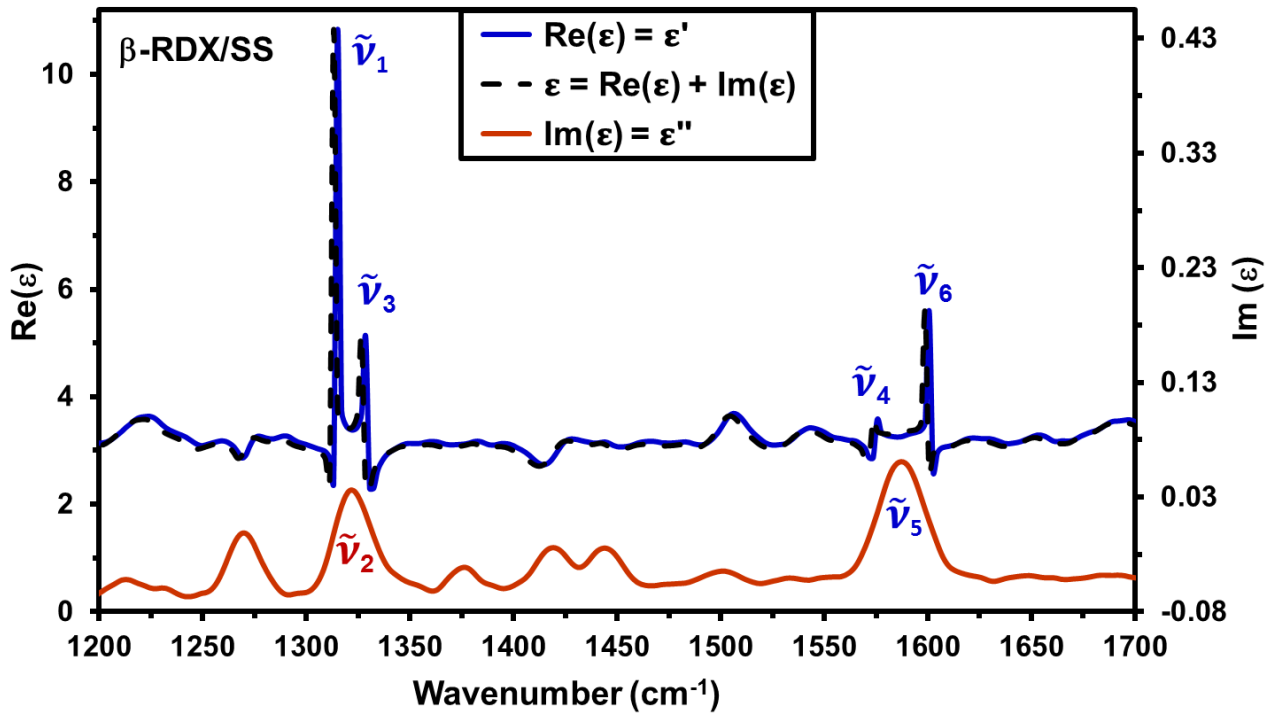

Figure 5. Permittivity (ε) of predominantly β-RDX crystalline films deposited on SS substrates (segmented black trace). The transversal optical function is expressed as the imaginary part [Im(ε̂); red trace] and real part [Re(ε̂); blue trace] of the permittivity.

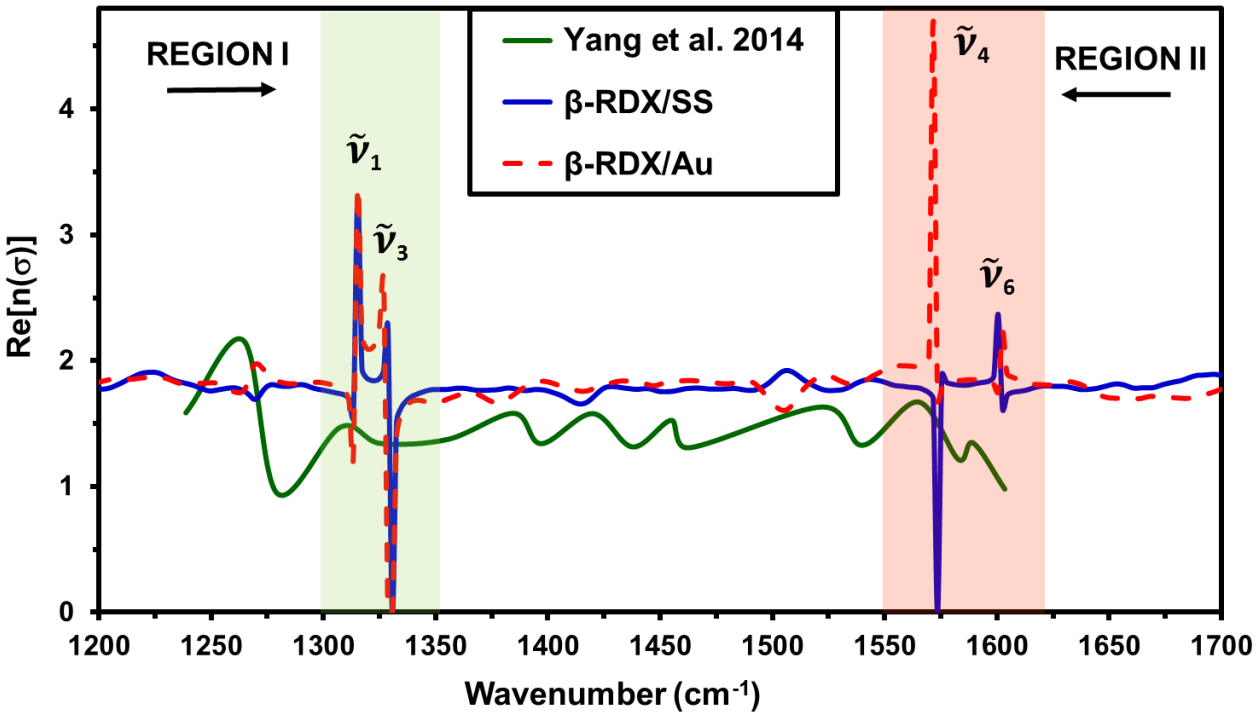

Figure 6. Comparison of the refractive index of RDX thin films from this contribution with literature values. RDX/ZnSe-ATR (Yang et al.[29]; green trace); β-RDX/SS (blue trace); β-RDX/Au (segmented red trace).

Table I. Maximum values of the refraction Index [$n(\tilde{\nu})$], extinction coefficient [$\kappa(\tilde{\nu})$], and absorption coefficient [$\alpha(\tilde{\nu})$] for predominantly β-RDX layers deposited on Au and SS

Substrate	$\tilde{\nu}$ (cm^{-1})	$k(\tilde{\nu})$	$\alpha(\tilde{\nu})$	$n(\tilde{\nu})$	Max Values (Fig. 6)
SS	1315.26	8.92×10^{-4}	1.475×10^{1}	3.29	Region I
SS	1321.04	8.30×10^{-3}	1.378×10^{2}	1.84	

SS	1328.76	2.29×10^{-3}	3.829×10^{1}	2.26	
Au	1315.26	2.34×10^{-2}	3.874×10^{2}	3.36	
Au	1322.97	1.20×10^{-1}	1.994×10^{3}	2.14	
Au	1326.83	6.52×10^{-2}	1.087×10^{3}	2.64	
SS	1575.61	2.85×10^{-3}	5.649×10^{1}	1.89	Region II
SS	1587.18	1.55×10^{-2}	3.089×10^{2}	1.80	
SS	1600.68	8.39×10^{-4}	1.688×10^{1}	2.37	
Au	1571.75	1.85×10^{-1}	3.678×10^{3}	1.85	
Au	1587.18	1.89×10^{-1}	3.777×10^{3}	1.85	
Au	1602.61	9.79×10^{-3}	1.971×10^{2}	2.23	

Table II. Maximum values of Im(ε) on Au and SS substrates obtained from data shown in Figures 4 and 5. Calculated values of conductivity (σ) and resistivity (ρ) for predominantly β-RDX layers deposited on the two substrates studied were found using Eq. 7

$\tilde{\nu}_2$ = 1321.0 cm^{-1} ↔ $\tilde{\nu}_{TO}$ = 3.97×10^{13} Hz				$\tilde{\nu}_5$ = 1587.2 cm^{-1} ↔ $\tilde{\nu}_{TO}$ = 4.76×10^{13} Hz			
Substrate	$\mathrm{Im}(\hat{\varepsilon}) = \varepsilon''$	σ $(ohm\cdot m)^{-1}$	ρ ohm·m	Substrate	$\mathrm{Im}(\hat{\varepsilon}) = \varepsilon''$	σ $(ohm\cdot m)^{-1}$	ρ ohm·m
Au	0.51	1.13×10^{3}	8.85×10^{-4}	Au	0.70	1.85×10^{3}	5.39×10^{-4}
SS	0.03	6.75×10^{1}	1.48×10^{-2}	SS	0.06	1.48×10^{2}	6.76×10^{-3}

Table III. Comparison of various experimental setups and conditions used to obtain the optical properties of RDX in the MIR region

Authors (yr)	Incident angle	Methodology / substrates	Technique	Thickness (h)	Source polarization
Isbell-Brewster (1998)	0°	FTIR / KBr pellet	Transmission	0.5 μm < h < 1 cm	None
Yang et al. (2014)	45°	ZnSe ATR*	Ellipsometry	< 20 μm	s and p
This work	80°	Au, SS	RAIRS	2 nm < h < 200 nm	s and p

*zinc selenide attenuated total reflectance

SUPPLEMENTAL MATERIAL

This section includes five figures: (1) RAIRS spectra excited with polarized light of predominantly β-RDX crystalline films on an Au substrate compared to spectrum with unpolarized light; (2) RAIRS spectra excited with polarized light of predominantly β-RDX crystalline films on SS substrate compared with spectrum acquired with unpolarized light; (3) imaginary part of the permittivity (ε) of predominantly β-RDX crystalline films deposited on (a) gold substrates, and (b) SS substrates; (4) extinction coefficient $\{k(\tilde{\nu}) = \mathrm{Im}[n(\tilde{\nu})]\}$ of predominantly β-RDX crystalline films deposited on Au and SS substrates; (5)

absorption coefficient [$\alpha(\tilde{\nu})$] of predominantly β-RDX crystalline films deposited on Au and SS substrates.

In Figure SM-1, solvent modes are indicated with solid black guide arrows, and the dashed red arrows represent vibrational modes corresponding to the solvent and/or of the α-RDX polymorph.

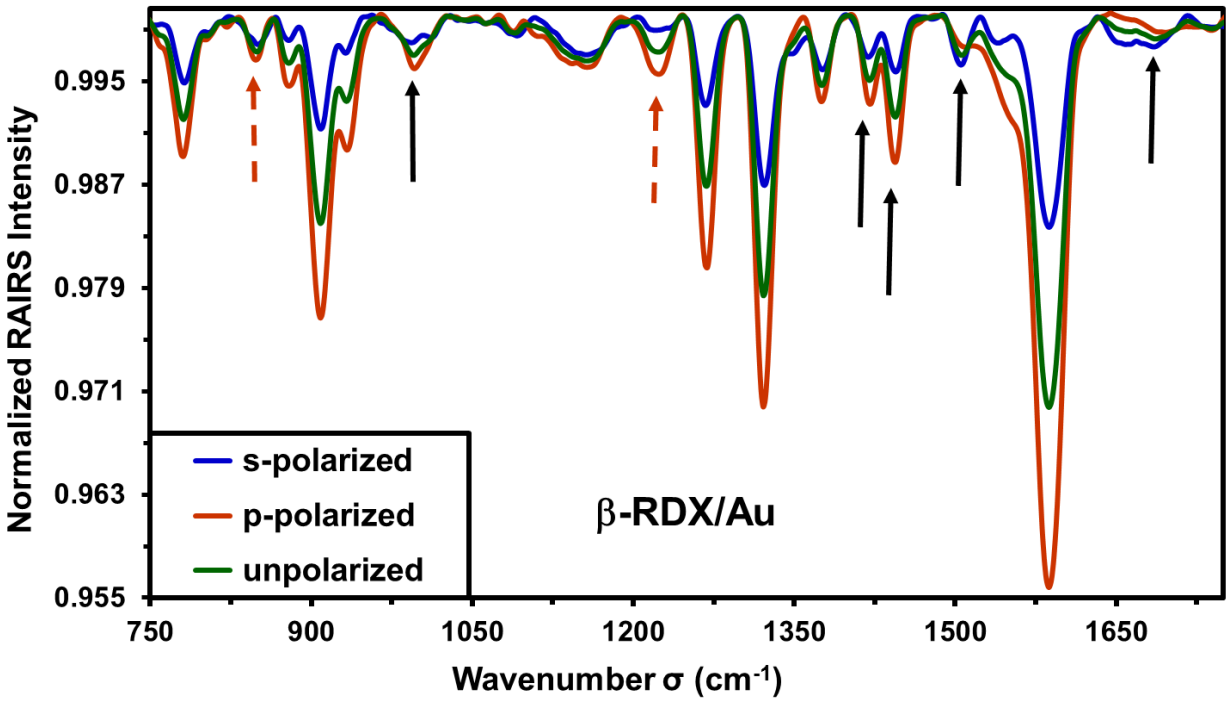

Figure SM-1. RAIRS spectra with excited with polarized light (s & p polarizations) of predominantly β-RDX crystalline films on Au substrate compared with spectra obtained with unpolarized light. Spectrum with s-polarized light is illustrated by the blue trace; spectrum acquired with p-polarized light is represented by the red trace, and spectrum with unpolarized light is shown as the green trace.

Figure SM-2, solvent bands are indicated with black solid arrow guidelines. The red dashed arrow guidelines represent vibrational modes corresponding to the solvent and very small amounts of the α-RDX polymorph. The same scales as in Figure SM-1 have been maintained for purposes of comparison of the intensities of the bands observed on the two substrates.

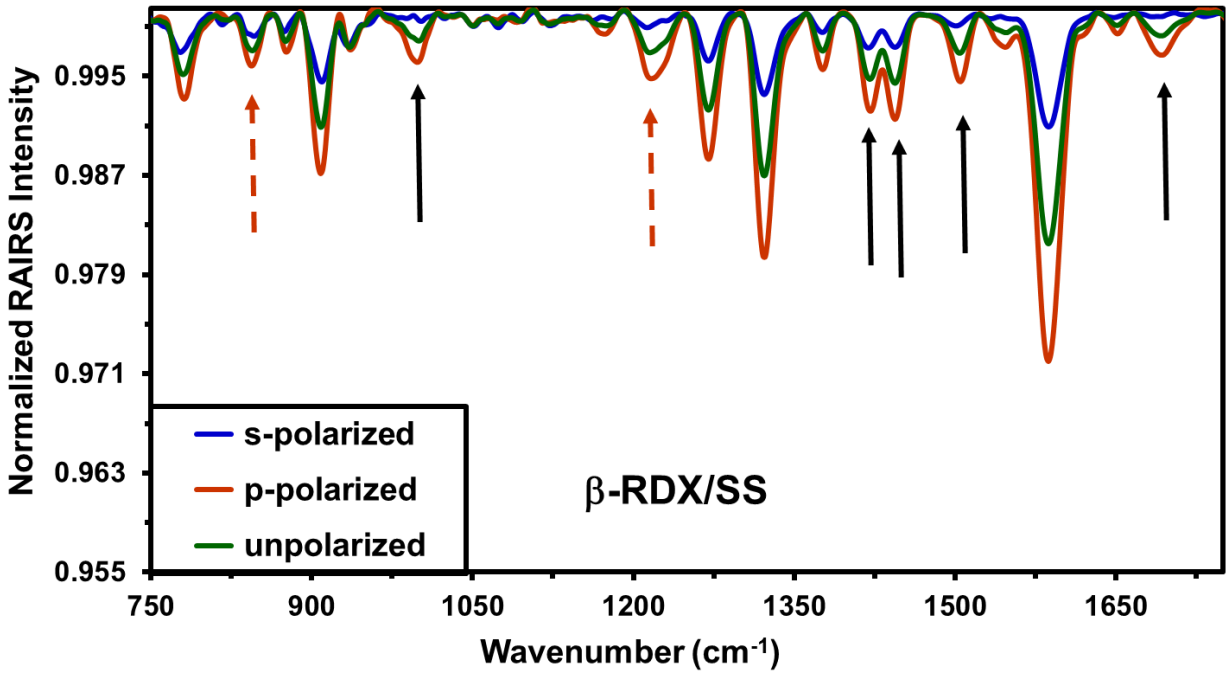

Figure SM-2. RAIRS spectra excited with polarized light (s & p polarizations) of predominantly β-RDX crystalline films on SS substrate compared with spectrum obtained with unpolarized light. Spectrum acquired with s-polarized light is illustrated by blue trace; spectrum excited with p-polarized light is represented by the red trace; spectrum obtained with unpolarized light is shown as green trace.

Figure SM-3 shows imaginary part of the permittivity (ε) of predominantly β-RDX crystalline films deposited on (a) gold substrates, and (b) SS substrates.

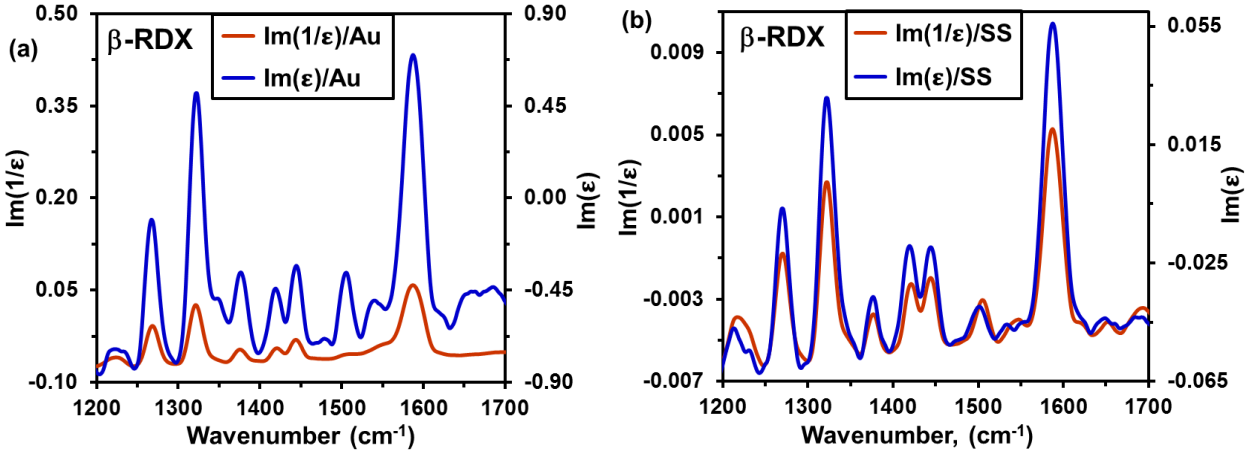

Figure SM-3. Imaginary part of the permittivity (ε) of predominantly β-RDX crystalline films deposited on (a) gold substrates, and (b) stainless steel substrates. The blue trace corresponds to the imaginary part of the inverse of permittivity (1/ε), and the red trace corresponds to the imaginary part of the permittivity (Im(ε); secondary "y" axis).

Figure SM-4 illustrates the extinction coefficient $\{k(\tilde{\nu}) = \mathrm{Im}[n(\tilde{\nu})]\}$ of predominantly β-RDX crystalline films deposited on Au and SS substrates and Figure SM-5 shows the absorption coefficient $[\alpha(\tilde{\nu})]$ of predominantly β-RDX crystalline films deposited on Au and SS substrates.

10.1177/0003702817710248

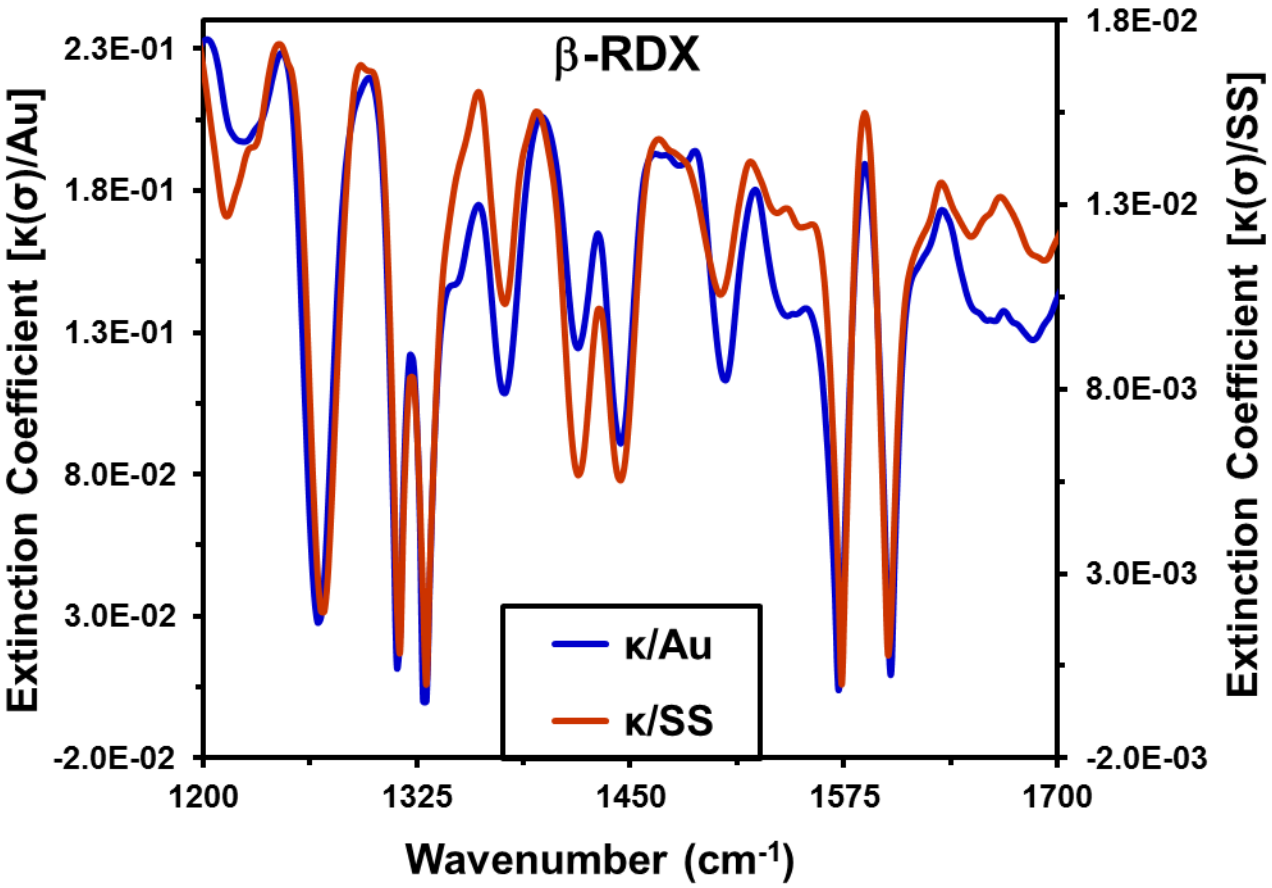

Figure MS-4. Extinction coefficient $[k(\tilde{\nu}) = \mathrm{Im}(n(\tilde{\nu}))]$ of predominantly β-RDX crystalline films deposited on Au (blue trace; principal "y" axis), and SS (red trace; secondary "y" axis).

10.1177/0003702817710248

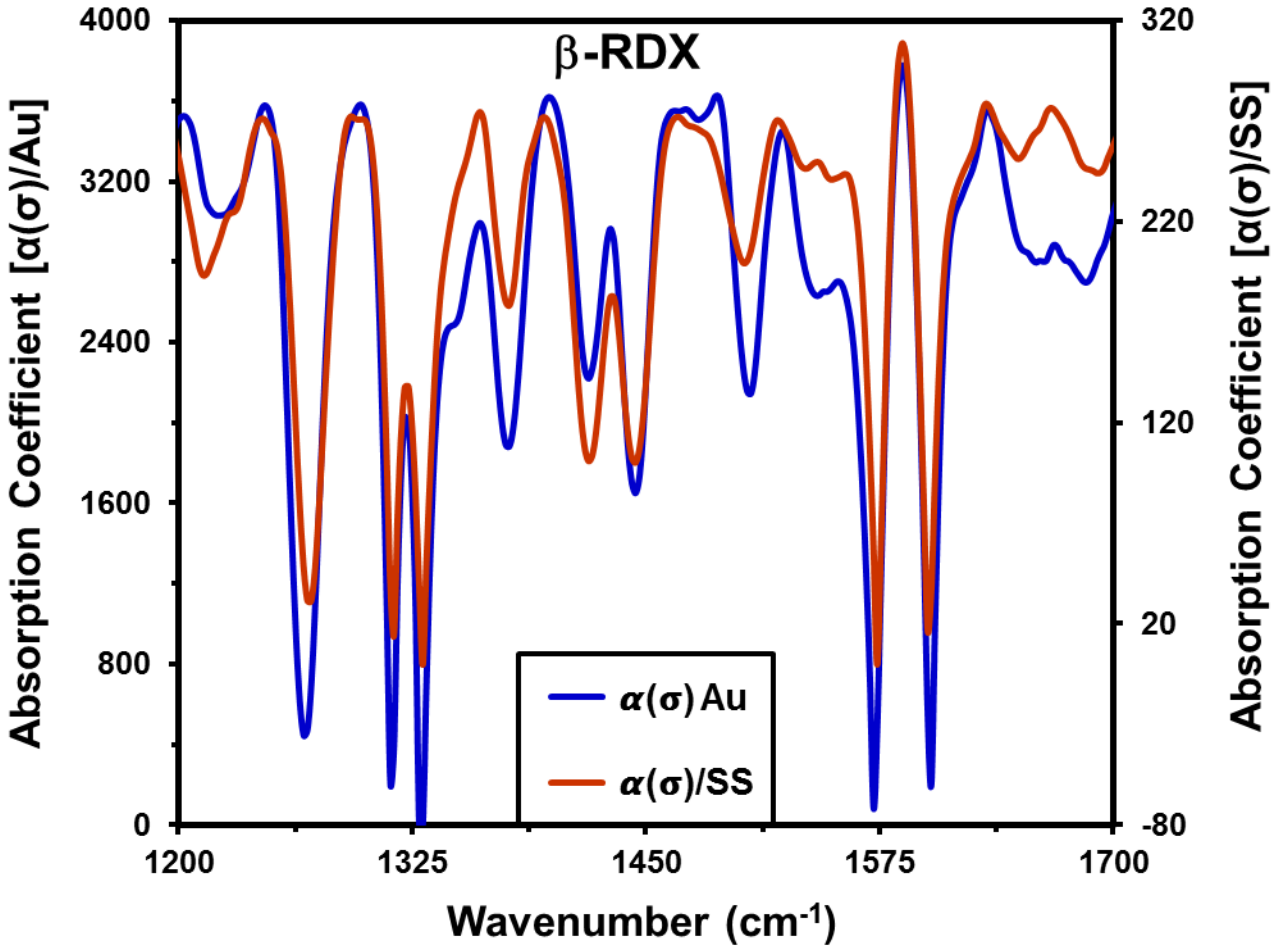

Figure SM-5. Absorption coefficient $[\alpha(\tilde{\nu})]$ of predominantly β-RDX crystalline films deposited on Au (blue trace; principal "y" axis), and SS (red trace; secondary "y" axis).